## Chapter 6

## *In vivo* response of Ca/Zr co-doped $MgSiO_3$ nanoparticles

*This chapter explores the in vivo potentiality that aims to assess both local and systemic toxicity of co-substitution of Ca and Zr in $MgSiO_3$ [$Mg_{1-x}Ca_xSi_{1-x}Zr_xO_3$ (x = 0 - 0.1, 0.2, 0.3, 0.4); MCSZO-X, X=0 – 4] nanoparticles using rat model. The cytotoxicity of MCSZO-X (X=0 – 4) nanoparticles was preliminarily evaluated by exposing MG-63 cells to varying concentrations as 0.25, 2.5, 25 mg/ml. Consequently, the biocompatibility of MCSZO-X nanoparticles was tested by injecting the eluates of concentration of 25 mg/ml into the synovial joints of rats for 7 days. Histological analyses were conducted on the organs, to detect the signs of inflammation. Furthermore, the biochemical assays (Alkaline phosphatase and Creatinine activities) were conducted on the extracted serum from the rats, subjected to particulate treatment.*

### 6.1. Phase analyses

Figure. 6.1. represents the XRD pattern of MCSZO-X (X = 0 - 4) nanoparticles. XRD pattern confirms the formation of monoclinic pure $MgSiO_3$ [JCPDS # 35-0610] phase with P21/c space group. In addition, a few minor peaks, indexed with JCPDS # 34-0189 with Pmnb space group. However, the peak shifted towards a lower angle with the incorporation of Ca and Zr with increasing the concentration from 0 to 0.3, as shown in Figure. 1b. Moreover, the crystallite size was calculated from Scherrer's formula [1, 2]. The crystallite size of prepared sample was decreased from 35 nm to 31 nm with an increase in the amount of Ca and Zr from 0 to 0.3. After that crystallite size again increases from 31 nm to 33 nm with increase in the amount of Ca and Zr, from 0.3 to 0.4. Figure.1b demonstrates that with increasing the concentration from 0 to 0.3, the peaks shifted towards lower 2 theta values from 28.24º to 28.08º.

With further increase in the concentration from 0.3 to 0.4, the peak shift towards the higher angle again from 28.08º to 28.33º, as represented by the enlarged view.

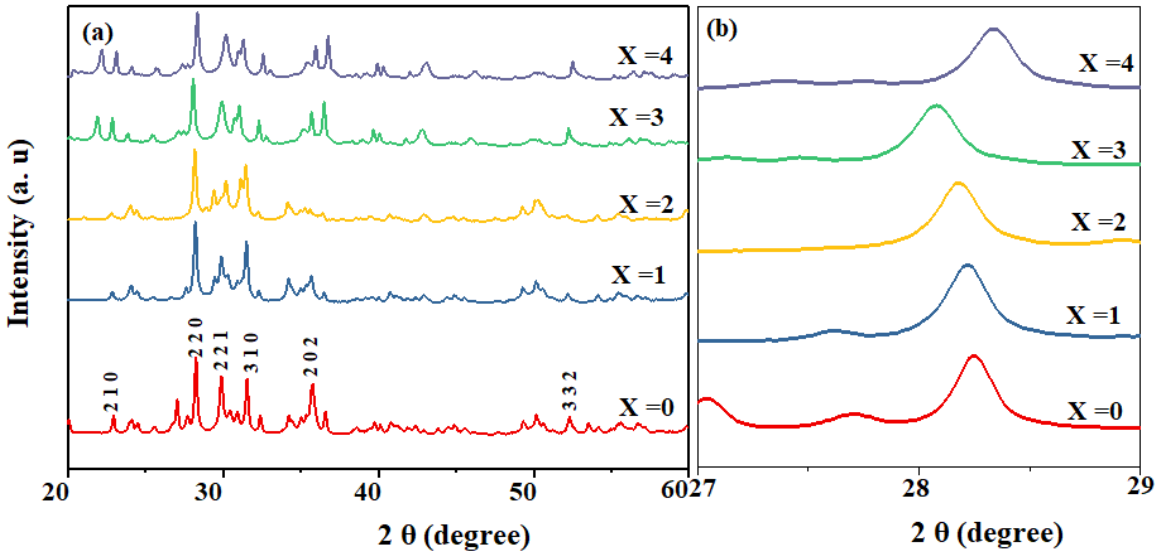


*Figure 6.1. XRD results of MCSZO-X (X = 0- 4)* nanoparticles. *(a) XRD patterns of different samples of MCSZO (X= 0 – 4) calcined at 1300º C for 10 h. (b) enlarged view of the highest intense peaks of samples.*

The FT-IR spectra of MCSZO-X nanoparticles confirmed the incorporation of Ca and Zr in $MgSiO_3$ structure, as shown in Figure. 6.2. The specific peaks of Si – O at 470, 500, 600, and 1052 $cm^{-1}$ corresponds to bending and stretching vibrations, respectively. The bending vibration observed at around 800 $cm^{-1}$ in Si-O-Si indicates the formation of $MgSiO_3$ [3, 4]. Moreover, the vibrational peak, representing Si-O within silicate tetrahedra, is observed at 682 $cm^{-1}$. Furthermore, the stretching and bending vibrations of Mg-O are associated with the vibrational bands at 517 $cm^{-1}$ and a peak close to 870 $cm^{-1}$ [5]. Additionally, the peaks at 1320 $cm^{-1}$ and 1127 $cm^{-1}$ correspond to the stretching vibrations of C=O and C-O, respectively [6].

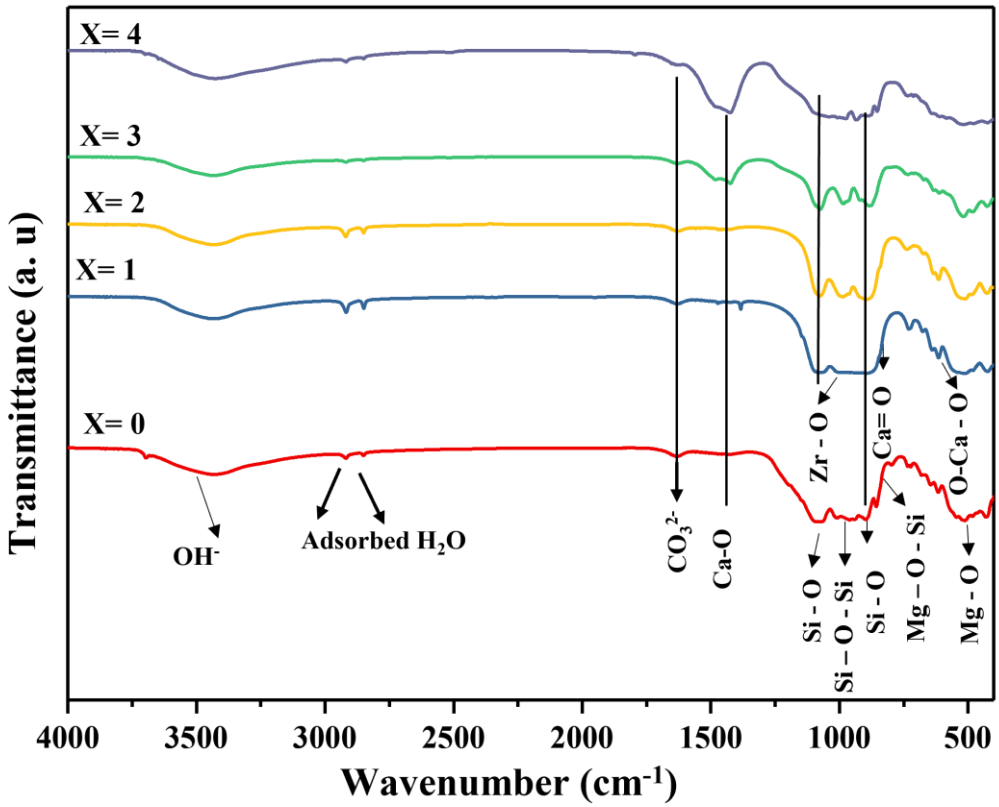


*Figure 6.2. FT-IR spectra of Ca- Zr doped $MgSiO_3$ (MCSZO-X, X = 0 - 4) nano powder.*

**6.2. Microstructural analyses**

Figure. 6.3. represents the microscopy images (high-resolution scanning electron, HRSEM) of MCSZO-X nanoparticles. The average particle size of MCSZO-X nano powder were increased (346, 377, 400, 418, 452nm) with increase in the amount of Ca and Zr from 0 to 4 in MCSZO-X.

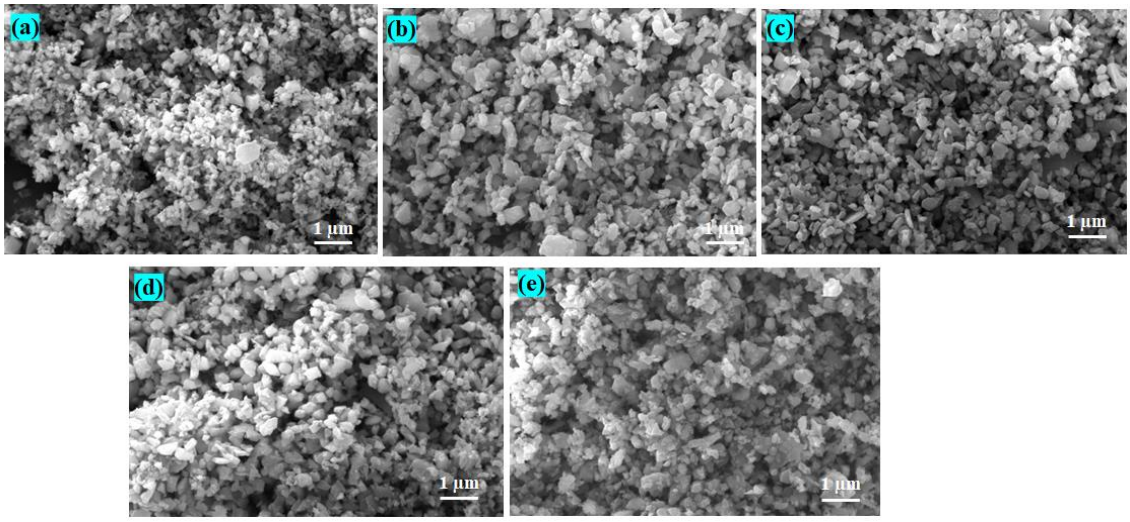


*Figure 6.3. Scanning electron micrographs of MCSZO-X* nanoparticles. *(a) X=0, (b) X= 1, (C) X= 2, (d) X=3 and (e) X=4.*

### 6.3. Leaching behavior

Figure. 6.4. illustrates the amount of $Ca^{2+}$, $Mg^{2+}$, $Si^{4+}$, and $Zr^{4+}$ ions, leached from different concentrations of MCSZO-X nanoparticles after 3, 5, and 7 days of immersion in saline. The leaching of $Mg^{2+}$, and $Si^{4+}$ ions from different nanoparticles (M1, M2, M3, M4, and M5) are lower in comparison to pure MCSZO-X (X = 0) nanoparticles as the concentration of $Mg^{2+}$ and $Si^{4+}$ decreases with increasing the concentration of $Ca^{2+}$ and $Zr^{4+}$ dopant. However, the leaching of $Ca^{2+}$ and $Zr^{4+}$ ions increases. In addition, the amount of $Ca^{2+}$, leached from MCSZO-X nanoparticles are also increased with increasing the immersion time from 5 to 7 days.

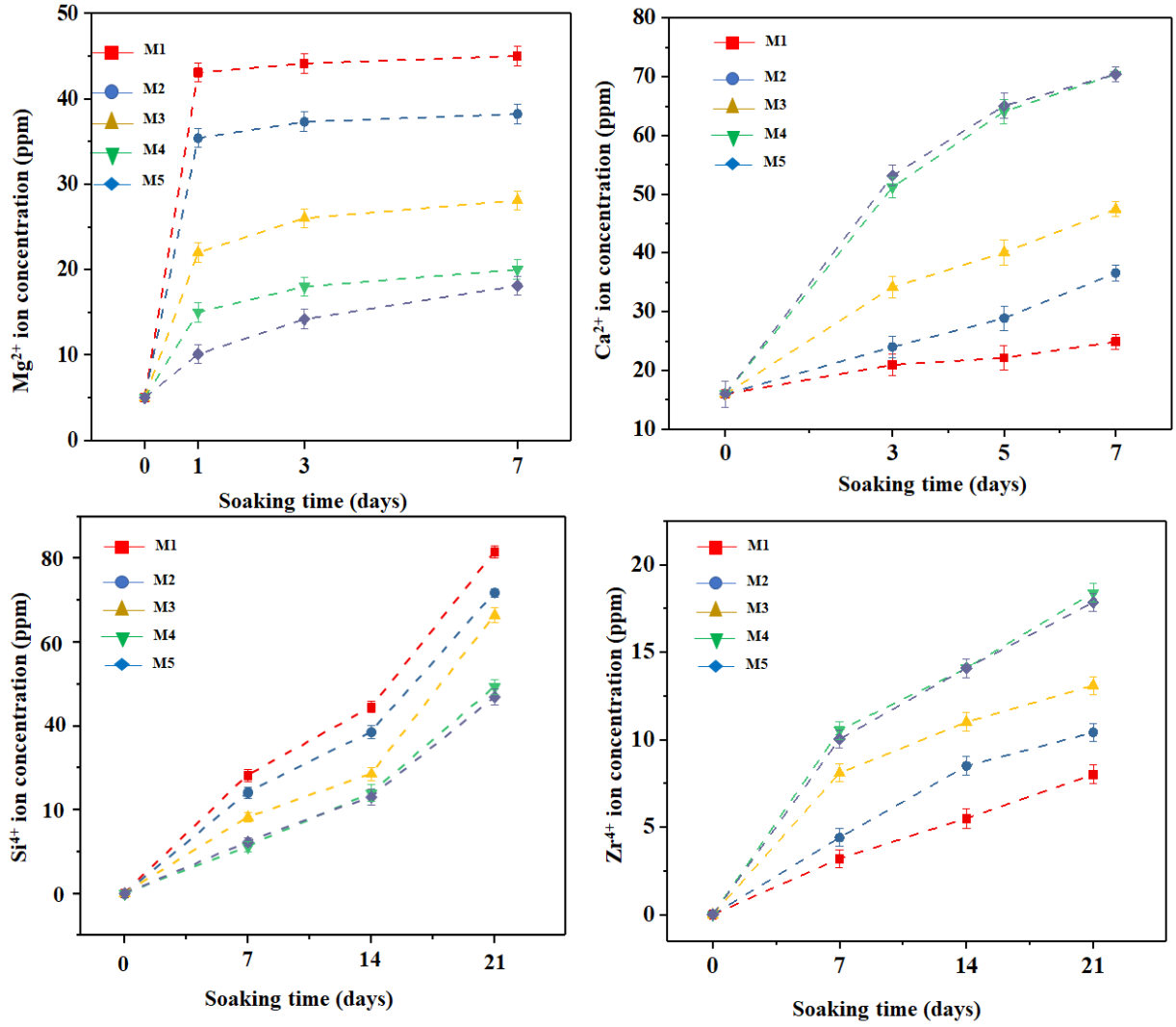


*Figure 6.4. Leaching behavior of $Mg^{2+}$, $Si^{4+}$, $Ca^{2+}$, and $Zr^{4+}$ from MCSZO- X (X = 0 - 4) nanoparticles in saline.*

### 6.4. Cell viability

The viability of MG-63 cells was evaluated using MTT assay at different elute concentrations (C1, C2, and C3 for M1, M2, M3, M4 and M5 samples). Figure 6.5. demonstrates the proliferation of MG-63 cells on prepared MCSZO-X nanoparticles, after 1 and 3 days. The viability of MG-63 cells, cultured on the MCSZO-X nanoparticles, was lower in comparison to the control after 1 day. However, when increasing the culture duration from day 1 to day 3, the viability of MG-63 cells, were increased with increasing the concentration of Ca and Zr in MCSZO-X nanoparticles.

Also, the elutes prepared at lower concentrations (0.25 mg/ml) demonstrates higher proliferation of MG-63 cells, cultured on MCSZO-X nanoparticles as compared to higher concentrations (2.5 and 25 mg/ml). These results suggested that with increasing the concentration the viability of the MCSZO-X nanoparticles decreases after 1 day of incubation. Therefore, after 3 days of culture the proliferation of MG-63 cells on MCSZO-X nanoparticles is significantly higher in comparison to control [Figure. 6.5]. It is noteworthy that cell viability is comparatively higher in eluates with high concentration of Ca and Zr such as MCSZO -3 and MCSZO - 4 when compared to eluates with lower concentrations of Ca and Zr containing MCSZO-X nanoparticles, after 3 days of incubation.

The asterisk symbol (*) indicates the significant variation in optical density across all MCSZO-X samples (M1, M2, M3, M4 and M5) at different concentrations in comparison to control, after 1 day of culture [Figure. 6.5 (a)]. However, symbol (#) shows the significant variation in the optical density across all MCSZO-X (M1, M2, M3, M4 and M5) nanoparticles, cultured for 3 days in comparison to the entire MCSZO-X samples, cultured with 24 h [Figure. 6.5 (b)].

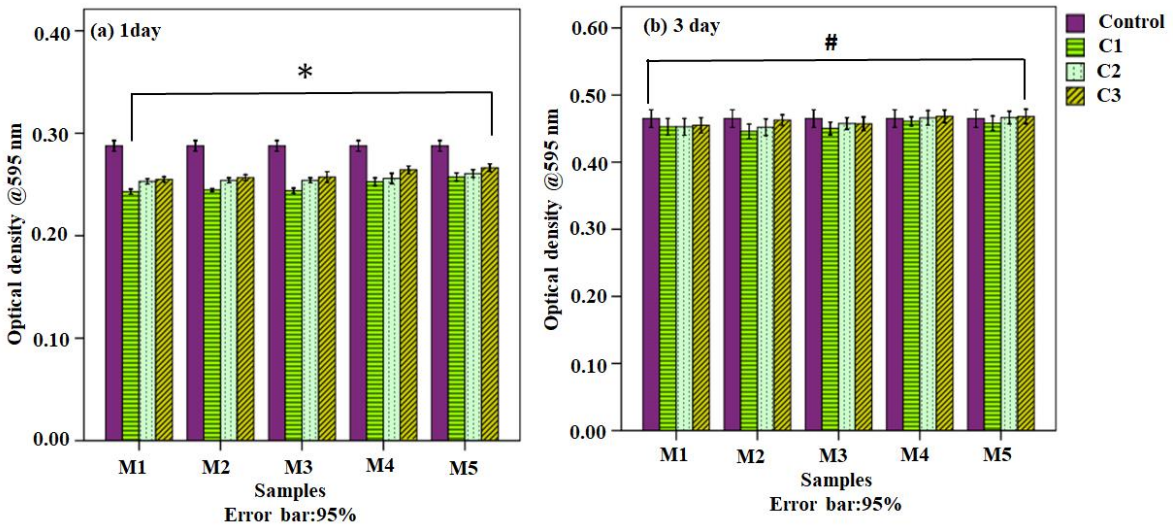


*Figure 6.5. Optical density of MG-63 cells, after the culture duration of 1 and 3 days, on MCSZO-X (X = 0−4); [M1, M2, M3, M4 and M5) nanoparticles at different concentration, i.e; 0.25, 2.5 and 25 mg/ml samples] and HA, used as a control.*

## 6.5. *In vivo* studies

### 6.5.1. General observation

After injecting the MCSZO-X particle for seven days, the skin texture and salivation of the rat remained unchanged. Also, after the intra-articular injection, the rats did not exhibit symptoms such as, diarrhea, tremor or convulsions. Additionally, after seven days of post-injection, no notable changes were observed in behavior of rats. Also, the injection site in every group of rats did not display any sign of inflammation (swelling or redness) throughout the observation period. Digital cameras were used to take paw photographs of the rats, treated with MCSZO-X particle injected group, which were then compared to the paw images of the control as well as saline-treated groups [Figure. 6.6].

The paws of the rats, injected with MCSZO-x nanoparticles (M1, M2, M3, M4 and M5), are similar to those of the saline-treated and control rats, revealing no indication of abnormalities, inflammation, redness, or edema.

Likewise, after completion of the experiment, the knee joints of the treated, control and saline, rats displayed unchanged morphology. Furthermore, as aforementioned, there was no inflammation detected at the injection site, and no signs of atrophy were noted in the adjacent bone structures such as the tibia and femur. This result corresponds with the *in vitro* cytocompatibility of MCSZO-X nanoparticles with varying concentration of Ca and Zr [Figure. 6.5].


*Figure 6.6. Digital camera images of rat paws before injection, on the 3rd day, and 7$^{th}$day after receiving injections of MCSZO-X nanoparticles into their knee joints.*

### 6.5.1.1. Impact of intra-articular injection of MCSZO-X on body weight

The variation in body weight is crucial for assessing whether injected nanoparticles have adversely affected the function of vital organs [7, 8]. Consequently, before and after (after 7 days) injection, the weight of each of the 35 rats was recorded. Rats in the control, saline, injected nanoparticle groups were not showing any significant changes in weight [Figure. 6.7]. Statistical analyses using two-way ANOVA showed no noticeable variation in body weight [9].

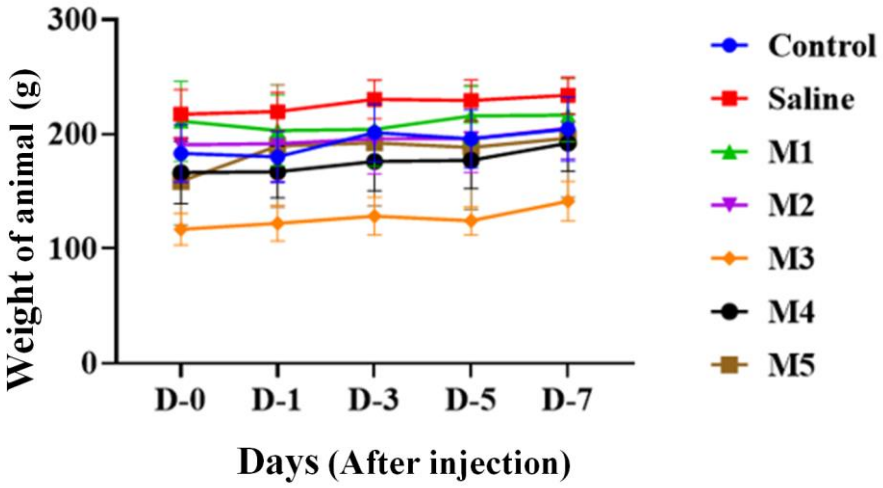


*Figure 6.7. The effect of intraarticular injection of MCSZO-X (M1, M2, M3, M4 and M5) nanoparticles on the body weight of rats throughout the experiment. All given values are in mean ± SD (n = 5 rats/group). (Two-way ANOVA showed no notable variation in the body weight of all rats).*

### 6.5.2. Hematological analyses

Changes in hematological parameters in humans and animals are indicative of drug-induced toxicity. The hemotopoietic system is a vital body system that produces the cellular blood components [9]. In this study, the effects of interarticularly injected MCSZO-X nanoparticles on the blood cells such as WBC and MCV were evaluated as compared to the control group (Figure. 6.8). The evaluation of basic hematological parameters, such as the measurement of

WBC and MCV is a crucial stage in the toxicity detection process. The statistical analyses using one-way ANOVA showed no significant variation in WBC ($p > 0.05$) among the all groups in MCSZO-X nanoparticles injected rats in comparison to the saline group [Figure. 6. 8(a)]. Also, there were no notable changes in the MCV ($p > 0.05$) among all the injected MCSZO-X nanoparticles groups as compared to the saline groups [Figure. 6. 8 (b)].

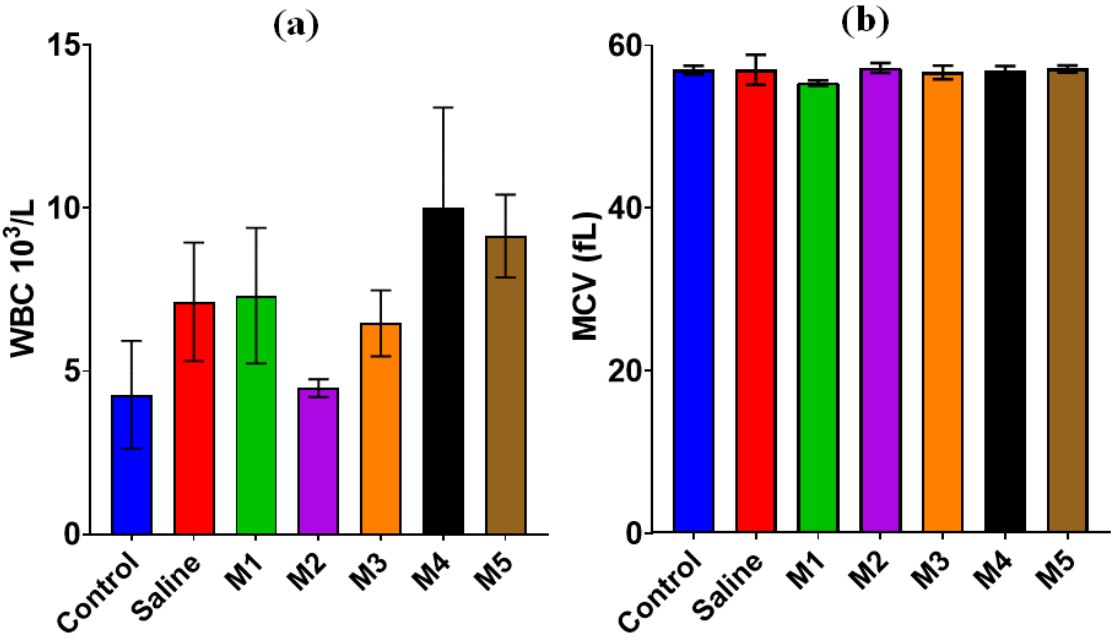


*Figure 6.8. Effect of intracticular injection of MCSZO-X nanoparticles in rats . (a) WBC count and (b) MCV on 7 day of injection. All given values are in mean ± SD (n = 5 rats per group).*

**6.5.3. Biochemical assays**

The impact of MCSZO-X nanoparticles (X = 0 - 4) on enzyme levels in rat blood was assessed by analyzing the biochemical properties of the extracted serum. Typically, the hepatic function is assessed by measuring the serum ALP activity level. The breakdown and restoration of liver tissue contribute to alteration in ALP activity [10, 11]. Additionally, hepatotoxicity raised by chemicals or drugs also increases the ALP activity in blood serum [12, 13]. As a result, the liver is an essential organ for examining the impact of toxicity

induced by nanoparticles. In this study, MCSZO-X nanoparticles were injected into the synovial joint. ALP, a marker of bone formation, plays an essential role in determining whether MCSZO-X nanoparticles exposure caused any bone abnormalities.

The statistical analyses reveals that there were no significant changes in serum levels (ALP) between the control and MCSZO-X nanoparticle treated (M0, M1, M2, M3 and M4) groups [Figure. 6.9 (a)].

Consequently, exposure to MCSZO-X nanoparticles did not alter liver function. Moreover, the assessment of serum creatinine levels is a typical method to detect potential adverse effects on renal function (Creatinine) caused by implant or foreign particles [14]. An elevated blood creatinine levels indicate reduced kidney filtration capacity [15-18]. In this study, the creatinine levels in the rat's blood serum, injected with M0, M1, M2, M3 and M4 nanoparticles, did not show any substantial differences in comparison to the saline group [Figure. 6. 9 (b)]. Also, the MCSZO-X nanoparticles did not lead to kidney impairment.

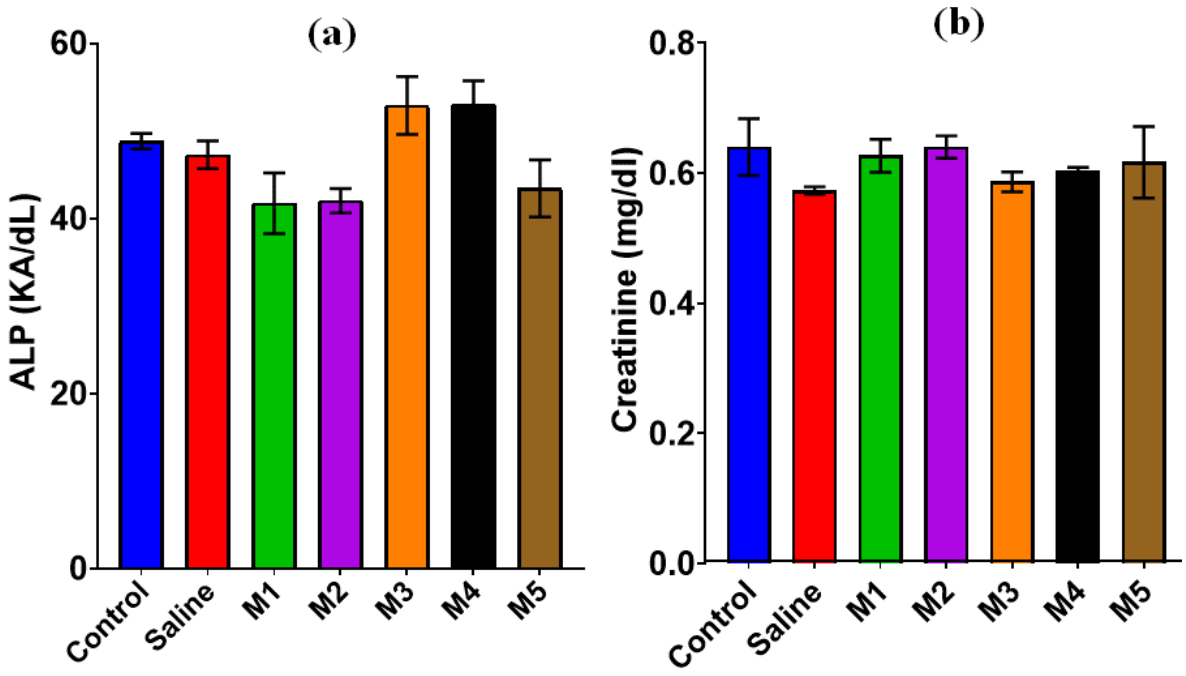


*Figure 6.9. Effect of MCSZO-X* nanoparticles *on serum concentration after 7 days of injection in rats. (a) ALP and (B) creatinine. All these values are in mean ± SD (n = 5 rats/group).*

**6.5.4. Histopathological analyses**

Over the period of seven days, it is possible that the nanoparticles, injected into the intraarticular region can enter the blood circulation and reached to organs like, liver, kidney, lung and heart as a result of regular physiological processes. Therefore, the histopathological analyses of the liver, heart, kidney and knee was done to determine the toxicity of MCSZO-X (X= 0- 4) nanoparticles. The comparison of histological images of various stained organ from particulate-injected groups (M1, M2, M3, M4, M5) with control and saline-injected groups are shown in Figures. 6.10 - 6.14. The sections of all the stained organs, in general, reveal that normal appearance and without presence of eluate particles. The MCSZO-X treated groups (M1, M2, M3, M4, and M5) did not reflect any sign of tissue shrinkage, cardiac muscle disorder, vacuolization, and bleeding. The muscle fibers appear straight and organized, resembling those in the control groups (Figure. 6.10).

The connective tissues of the hearts in the groups of rats, treated with particulates, exhibit normal architecture. In number of studies, it has been observed that exposure to fine concentrated particles can result in irregular beat and, in some cases, cardiac dysfunction [19-23].

The injection of $TiO_2$ nanoparticles has been shown to swell the endothelial cells of the heart, after 7 days [24]. In this study, the hearts of the rats in the M1, M2, M3, M4 and M5 eluates treated groups did not exhibit enlarged endothelial cells [Figure. 6.10]. Overall, the cardiac tissues of the rats treated with MCSZO-X (M1, M2, M3, M4 and M5) reveal no histopathological changes.

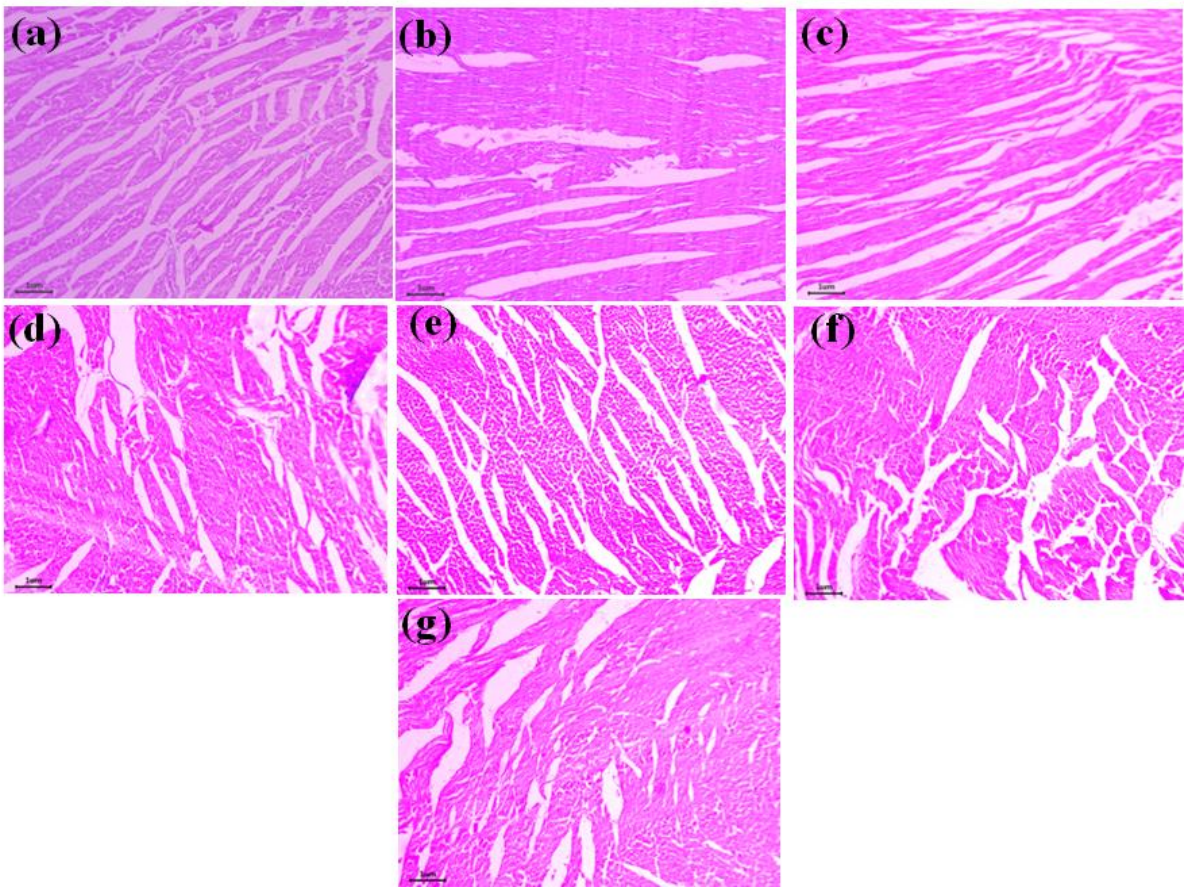


*Figure 6.10. Histopathological images of the heart tissues, stained with H & E after 7 days of injection in the following groups of rats: (a) Control (non-injected), (b) Saline, (c) M1, (d) M2, (e) M3, (f) M4 and (g) M5* nanoparticles *eluates treated groups (Scale bar: 1 µm)*

Evidently, the kidney is the main organ of the body to remove foreign nanoparticles [25]. As, the kidney removes foreign substances from the body by filtering, it is crucial for the kidney to take part to release of nanoparticles if they reach to the vital organs. Besides, the histopathology analyses of kidney's tissue is crucial for both identifying the nanoparticles and determining that how they may affect the structure and functioning of the kidneys. According to a number of studies, exposure to different nanoparticles like ZnO, Au, and $TiO_2$ causes pathological alterations in the kidney, including necrosis, dispersed glomeruli, and tubular dilatation [24, 26-28]. However, in comparison to control rat groups, the histopathological images of the kidney sections of rats injected with MCSZO-X particles (M1, M2, M3, M4 and M5) show unchanged renal tubules within the cortex (absence of any indication of vacuolar degeneration) [Figure. 6.11].

The kidney sections of rats, treated with control and MCSZO-X groups show normal renal cortex and glomerular cells without tubule dilation. Overall, histology of kidney sections reveal that the intra-articularly injected MCSZO-X nanoparticles (M1, M2, M3, M4 and M5) has no adverse effect on the kidney.

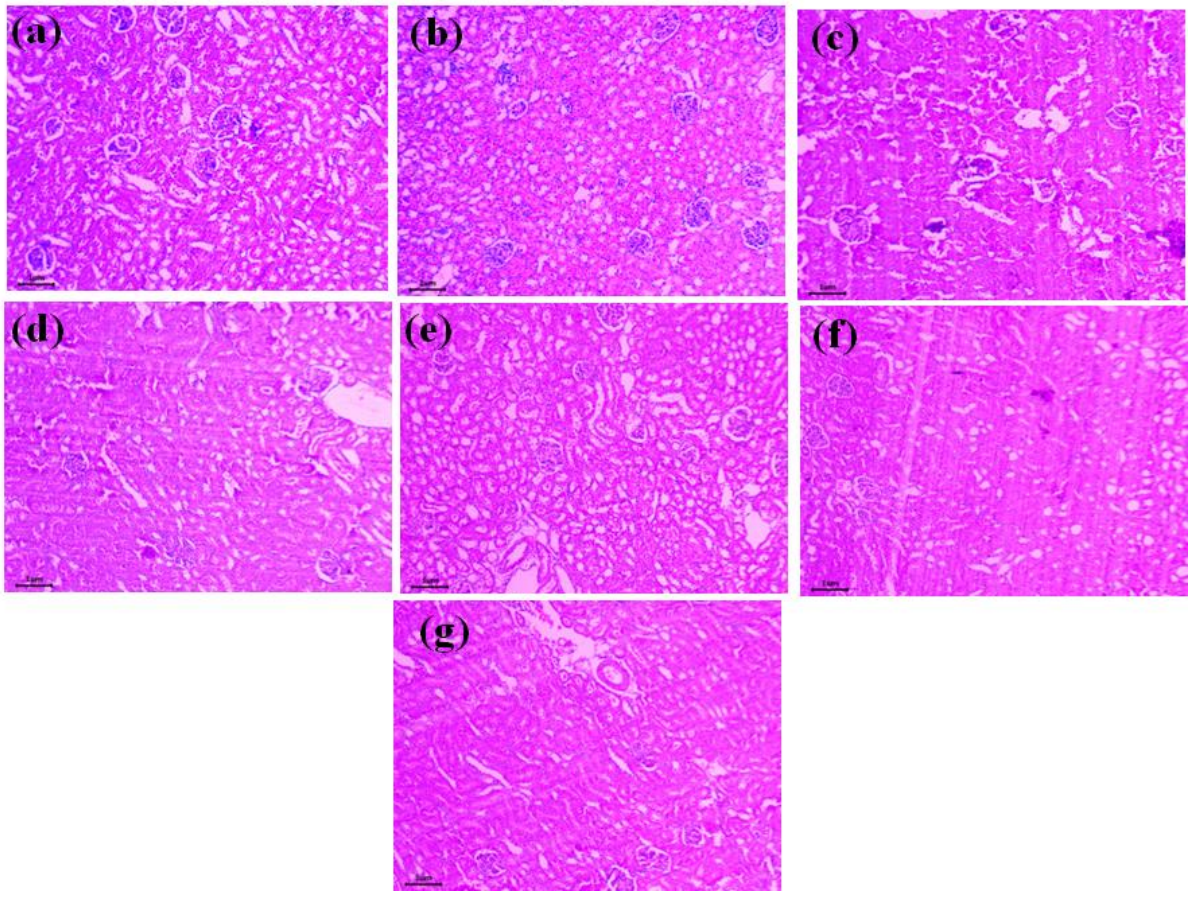


*Figure 6.11. Histopathological images of the kidney tissues, stained with H & E after 7 days of injection in the following groups of rats: (a) Control (non-injected), (b) Saline, (c) M1, (d) M2, (e) M3, (f) M4 and (g) M5* nanoparticles *eluates treated groups (Scale bar: 1 µm)*

The liver is one of the important organ that plays a main role in detoxifying the body. This means that it is possible for the foreign particles to move through the circulatory or lymphatic systems and into the liver [29-31].

Cytoplasmic vacuolization causes a disruption in the function of the membrane and can occasionally be a sign of liver injury [32-34]. In this study, there is no evidence of any vacuolization in cytoplasm of hepatocytes in the livers of the rats, treated with MCSZO-X nanoparticles. As a result, histological features of liver cells, injected with MCSZO-X particles (M1, M2, M3, M4 and M5) revealed no indications of any damage, bleeding, or necrosis near the sinusoids, when compared to those of control and saline rats [Figure. 6.12].

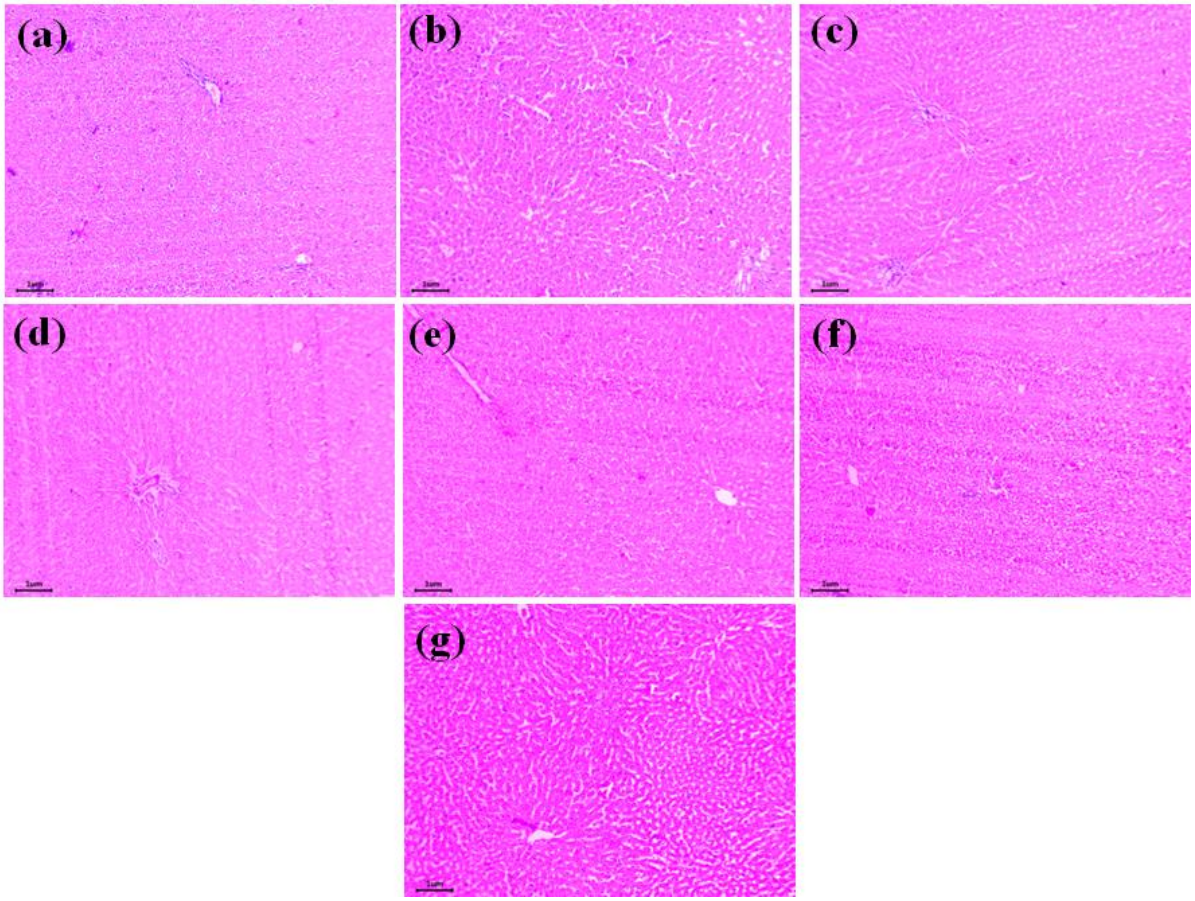


*Figure 6.12. Histopathological images of the liver section, stained with H & E after 7 days of injection in the following groups of rats: (a) Control (non-injected), (b) Saline, (c) M1, (d) M2, (e) M3, (f) M4 and (g) M5 nanoparticles eluates treated groups (Scale bar: 1 µm).*

Overall, the histopathological images of the organs stained with H & E of the M1, M2, M3, M4 and M5 injected nanoparticles reveal normal appearance and a comparable to that of the control and saline groups. The major organs of the rats of the nanoparticle treated groups show no evidence of particle dissemination.

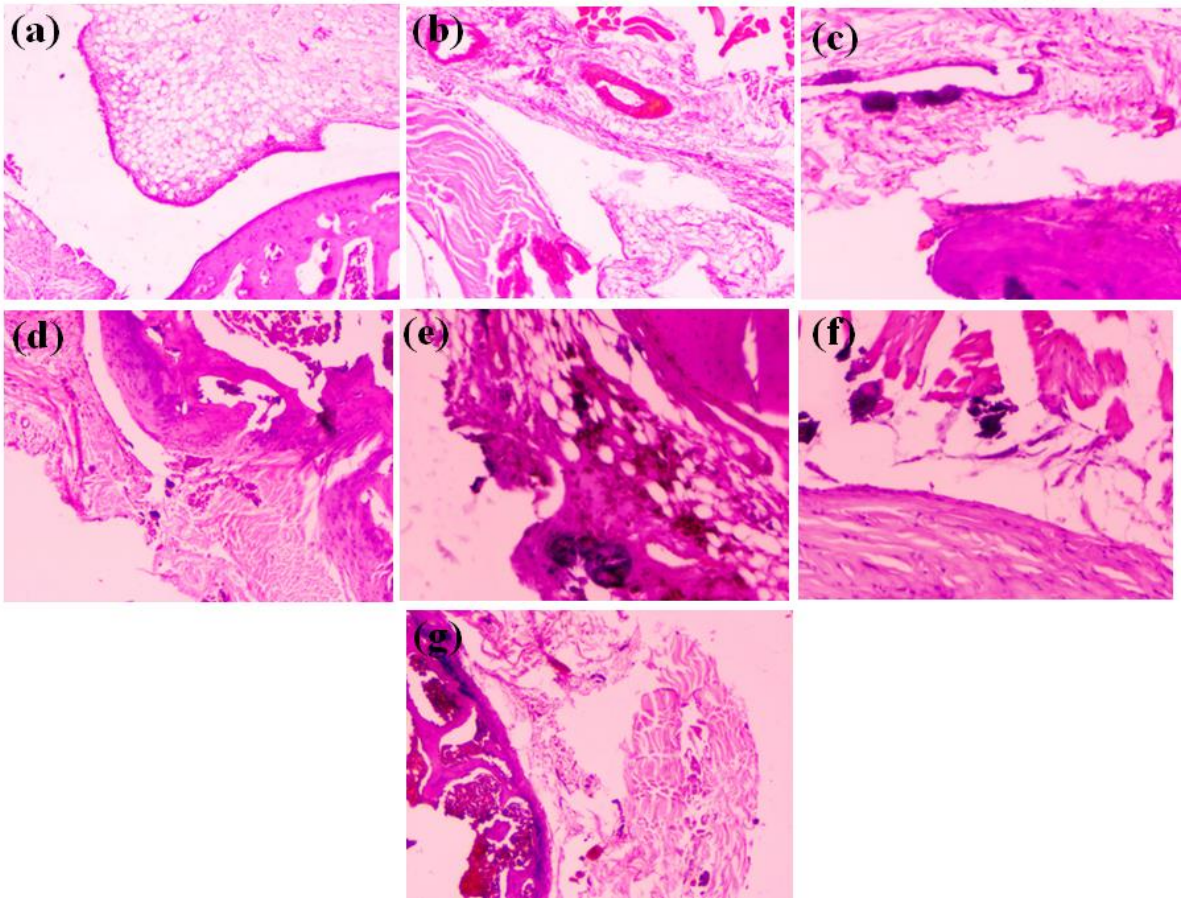


*Figure 6.13. Histopathological features of rat knee joint tissue, stained with H & E of intra-articular injection after 7 days in the following groups of rats: (a) Control (non-injected), (b) Saline, (c) M1, (d) M2, (e) M3, (f) M4 and (g) M5 nanoparticles eluates treated groups ( magnification: 40 X).*

The histological images provide a clear indication of the presence of nanoparticles within the fibroadipose tissue surrounding the synovial joint [Figure.6.13 (a–e)]. Moreover, the absence of macrophage infiltration can be clearly seen [Figure.6.13 (c-e)], which suggests the biocompatible nature of the prepared MCSZO-X nanoparticles [35, 36]. Furthermore, the administration of MCSZO-X nanoparticles via intra-articular injection did not lead to any damage to the cartilage or excessive growth of the synovial membrane.

The thickening of the synovial membrane, which occurs due to an increased density of cells resulting from the influx of different cell types [37-39].

The histological analyses of the knee joint did not reveal any negative response to the intra-articular administration of MCSZO-X nanoparticles. The histological analyses of rats treated with MCSZO-X (M1, M2, M3, M4 and M5) nanoparticles show no signs of inflammation at the implantation site of injection (synovial joint) or in vital organs [see in Figures. 6.13]. Moreover, MCSZO-X nanoparticles promote the proliferation of MG-63 cells [see Figure. 6.6]. Overall, MCSZO-X nanoparticles demonstrate *in vitro* cytocompatibility and *in vivo* biocompatibility.

In ceramic based implants the wear debris particles such as, $Al_2O_3$ and $ZrO_2$ are typically submicron in size [40, 41]. Earlier studies has been reported macrophages engulf submicron-sized particles, which increases the risk of an adverse reaction or inflammation [42-44]. However, histological images of knee joints treated with MCSZO-X nanoparticle showed no signs of macrophage infiltration (Fig. 13(c-f)), suggesting that MCSZO-X nanoparticles are biocompatible.

**6.6. Closure**

This chapter presents the assessment of *in vitro* and *in vivo* biocompatibility of pure $MgSiO_3$ and Ca and Zr co-doped $MgSiO_3$ nanoparticles with MG-63 cells and Rat model, respectively. Initial investigation indicates that $Mg_{1-x}Ca_xSi_{1-x}Zr_xO_3$ (x = 0, 0.1, 0.2, 0.3 and 0.4) nanoparticles promote the proliferation of MG-63 cells up to concentration of 25 mg/ml. The *in vivo* assessment revealed that the nanoparticles intraarticularly injected into the rats did not migrate to any of the major organs, including the kidney, heart and liver. In addition, the non-toxicity of MCSZO-X nanoparticles has been established by histological analyses of the knee and vital organs of rats, exposed to nanoparticle eluates with concentrations as 0.25, 2.5 and 25 mg/ml. Also, the absence of nanoparticles within the essential organs suggests that they were not transported to any of these organs. The histology of knee tissues of the rats, treated with nanoparticles, reveal the absence of any indications of inflammation.

Furthermore, biochemical parameters (ALP and creatinine) revealed that MCSZO - X nanoparticles had no toxic effect on functioning of vital organs.

**Bibliography**


[1] Cullity B D 1956 *Elements of X-ray Diffraction*: Addison-Wesley Publishing)

[2] Londoño-Restrepo S M, Jeronimo-Cruz R, Millán-Malo B M, Rivera-Muñoz E M and Rodriguez-García M E 2019 Effect of the nano crystal size on the X-ray diffraction patterns of biogenic hydroxyapatite from human, bovine, and porcine bones *Scientific reports* **9** 5915

[3] Choi C K 2010? Comparison between SiOC Thin Film by plasma enhance chemical vapor deposition and SiO2 Thin Film by Fourier Transform Infrared Spectroscopy? *Journal of the Korean Physical Society* **56** 1150-5

[4] Vancea C, Mihailescu M, Negrea A, Mosoarca G, Ciopec M, Duteanu N, Negrea P and Minzatu V 2020 Batch and fixed-bed column studies on palladium recovery from acidic solution by modified MgSiO3 *International Journal of Environmental Research and Public Health* **17** 9500

[5] Sagadevan S, Venilla S, Marlinda A, Johan M, Wahab Y A, Zakaria R, Umar A, Hegazy H H, Algarni H and Ahmad N 2020 Effect of synthesis temperature on the morphologies, optical and electrical properties of MgO nanostructures *Journal of nanoscience and nanotechnology* **20** 2488-94

[6] Kumar P, Dehiya B S, Sindhu A, Kumar R, Pruncu C I and Yadav A 2020 Fabrication and characterization of silver nanorods incorporated calcium silicate scaffold using polymeric sponge replica technique *Materials & Design* **195** 109026

[7] El Hilaly J, Israili Z H and Lyoussi B 2004 Acute and chronic toxicological studies of Ajuga iva in experimental animals *Journal of ethnopharmacology* **91** 43-50

[8] Bailey S A, Zidell R H and Perry R W 2004 Relationships between organ weight and body/brain weight in the rat: what is the best analytical endpoint? *Toxicologic pathology* **32** 448-66

[9] Buesen R, Landsiedel R, Sauer U G, Wohlleben W, Groeters S, Strauss V, Kamp H and van Ravenzwaay B 2014 Effects of SiO 2, ZrO 2, and BaSO 4 nanomaterials with or without surface functionalization upon 28-day oral exposure to rats *Archives of toxicology* **88** 1881-906

[10] Kaplan M M and Righetti A 1970 Induction of rat liver alkaline phosphatase: the mechanism of the serum elevation in bile duct obstruction *The Journal of clinical investigation* **49** 508-16

[11] Gawlik Z, Fiejka E, Aleksandrowicz R and Wiśniewska I 1978 Activity of alkaline phosphatase in the healing rat liver after hepatectomy *Folia Histochemica et Cytochemica* **16** 343-9

[12] Wright T M and Vandenberg A M 2007 Risperidone-and quetiapine-induced cholestasis *Annals of Pharmacotherapy* **41** 1518-23

[13] Singh A, Bhat T and Sharma O 2011 Clinical biochemistry of hepatotoxicity *J Clinic Toxicol S* **4** 2161-0495

[14] Panda N 1999 Kidney in: Textbook of Biochemistry and Human biology *Prentise Hall India* 290-6

[15] Chan P, O'hara G and Hayes A W 1982 Principles and methods for acute and subchronic toxicity *Principles and methods of toxicology* **12** 17-9

[16] Adefemi O, Elujoba A and Odesanmi W 1988 Evaluation of the toxicity potential of Cassia podocarpa with reference to official Senna *West Afr J Pharmacol Drug Res* **8** 41-8

[17] Oh R C and Hustead T R 2011 Causes and evaluation of mildly elevated liver transaminase levels *American family physician* **84** 1003-8

[18] Ene-ojo A S, Chinedu E A and Yakasai F M 2013 Toxic Effects of Sub-Chronic Administration of Chloroform Extract of Artemisia maciverae Linn on the Kidney of Swiss Albino Rats

[19] Timonen K L, Vanninen E, De Hartog J, Ibald-Mulli A, Brunekreef B, Gold D R, Heinrich J, Hoek G, Lanki T and Peters A 2006 Effects of ultrafine and fine particulate and gaseous air pollution on cardiac autonomic control in subjects with coronary artery disease: the ULTRA study *Journal of exposure science & environmental epidemiology* **16** 332-41

[20] Rich D Q, Zareba W, Beckett W, Hopke P K, Oakes D, Frampton M W, Bisognano J, Chalupa D, Bausch J and O'Shea K 2012 Are ambient ultrafine, accumulation mode, and fine particles associated with adverse cardiac responses in patients undergoing cardiac rehabilitation? *Environmental health perspectives* **120** 1162-9

[21] Peters A, Hampel R, Cyrys J, Breitner S, Geruschkat U, Kraus U, Zareba W and Schneider A 2015 Elevated particle number concentrations induce immediate changes in heart rate variability: a panel study in individuals with impaired glucose metabolism or diabetes *Particle and fibre toxicology* **12** 1-11

[22] Brook R D, Brook J R, Urch B, Vincent R, Rajagopalan S and Silverman F 2002 Inhalation of fine particulate air pollution and ozone causes acute arterial vasoconstriction in healthy adults *Circulation* **105** 1534-6

[23] Hamanaka R B and Mutlu G M 2018 Particulate matter air pollution: effects on the cardiovascular system *Frontiers in endocrinology* **9** 680

[24] Wang J-X, Fan Y-B, Gao Y, Hu Q-H and Wang T-C 2009 TiO2 nanoparticles translocation and potential toxicological effect in rats after intraarticular injection *Biomaterials* **30** 4590-600

[25] Ding T, Xue Y, Lu H, Huang Z and Sun J 2012 Effect of particle size of hydroxyapatite nanoparticles on its biocompatibility *IEEE transactions on nanobioscience* **11** 336-40

[26] Ibrahim K E, Al-Mutary M G, Bakhiet A O and Khan H A 2018 Histopathology of the liver, kidney, and spleen of mice exposed to gold nanoparticles *Molecules* **23** 1848

[27] Yan G, Huang Y, Bu Q, Lv L, Deng P, Zhou J, Wang Y, Yang Y, Liu Q and Cen X 2012 Zinc oxide nanoparticles cause nephrotoxicity and kidney metabolism alterations in rats *Journal of Environmental Science and Health, Part A* **47** 577-88

[28] Noori A, Karimi F, Fatahian S and Yazdani F 2014 Effects of zinc oxide nanoparticles on renal function in mice *International Journal of Biosciences (IJB)* **5** 140-6

[29] Lipka J, Semmler-Behnke M, Sperling R A, Wenk A, Takenaka S, Schleh C, Kissel T, Parak W J and Kreyling W G 2010 Biodistribution of PEG-modified gold nanoparticles following intratracheal instillation and intravenous injection *Biomaterials* **31** 6574-81

[30] Husain M, Wu D, Saber A T, Decan N, Jacobsen N R, Williams A, Yauk C L, Wallin H, Vogel U and Halappanavar S 2015 Intratracheally instilled titanium dioxide nanoparticles translocate to heart and liver and activate complement cascade in the heart of C57BL/6 mice *Nanotoxicology* **9** 1013-22

[31] Modrzynska J, Mortensen A, Berthing T, Ravn-Haren G, Szarek J, Saber A T and Vogel U 2021 Effect on mouse liver morphology of CeO2, TiO2 and carbon black nanoparticles translocated from lungs or deposited intravenously *Applied Nano* **2** 222-41

[32] Abdelhalim M A K and Jarrar B M 2011 Gold nanoparticles administration induced prominent inflammatory, central vein intima disruption, fatty change and Kupffer cells hyperplasia *Lipids in health and disease* **10** 1-6

[33] Abdelhalim M A K and Jarrar B M 2011 Gold nanoparticles induced cloudy swelling to hydropic degeneration, cytoplasmic hyaline vacuolation, polymorphism, binucleation, karyopyknosis, karyolysis, karyorrhexis and necrosis in the liver *Lipids in Health and Disease* **10** 1-6

[34] Abdelhalim M A K 2011 Gold nanoparticles administration induces disarray of heart muscle, hemorrhagic, chronic inflammatory cells infiltrated by small lymphocytes, cytoplasmic vacuolization and congested and dilated blood vessels *Lipids in health and disease* **10** 1-9

[35] Sheikh Z, Brooks P J, Barzilay O, Fine N and Glogauer M 2015 Macrophages, foreign body giant cells and their response to implantable biomaterials *Materials* **8** 5671-701

[36] Xia Z and Triffitt J T 2006 A review on macrophage responses to biomaterials *Biomedical materials* **1** R1

[37] Sergijenko A, Roelofs A J, Riemen A H and De Bari C 2016 Bone marrow contribution to synovial hyperplasia following joint surface injury *Arthritis Research & Therapy* **18** 1-11

[38] Asif Amin M, Fox D A and Ruth J H 2017 Synovial cellular and molecular markers in rheumatoid arthritis. In: *Seminars in immunopathology*: Springer) pp 385-93

[39] Burke C J, Alizai H, Beltran L S and Regatte R R 2019 MRI of synovitis and joint fluid *Journal of Magnetic Resonance Imaging* **49** 1512-27

[40] Lerouge S, Huk O, Yahia L H and Sedel L 1996 Characterization of in vivo wear debris from ceramic—ceramic total hip arthroplasties *Journal of Biomedical*

*Materials Research: An Official Journal of The Society for Biomaterials and The Japanese Society for Biomaterials* **32** 627-33

[41] Hatton A, Nevelos J, Nevelos A, Banks R, Fisher J and Ingham E 2002 Alumina–alumina artificial hip joints. Part I: a histological analysis and characterisation of wear debris by laser capture microdissection of tissues retrieved at revision *Biomaterials* **23** 3429-40

[42] Margevicius K J, Bauer T W, McMahon J T, Brown S A and Merritt K 1994 Isolation and characterization of debris in membranes around total joint prostheses *JBJS* **76** 1664-75

[43] Yang S-Y, Ren W, Park Y, Sieving A, Hsu S, Nasser S and Wooley P H 2002 Diverse cellular and apoptotic responses to variant shapes of UHMWPE particles in a murine model of inflammation *Biomaterials* **23** 3535-43

[44] Thrivikraman G, Madras G and Basu B 2014 In vitro/in vivo assessment and mechanisms of toxicity of bioceramic materials and its wear particulates *RSC Advances* **4** 12763-81